Spectroscopic and Theoretical Studies on the Reactions of Laser-Ablated Tantalum with Carbon Dioxide

Xue-Feng Wang, Mo-Hua Chen, Lu-Ning Zhang, and Qi-Zong Qin*

Laser Chemistry Institute, Fudan University, Shanghai 200433, China

Received: August 5, 1999; In Final Form: November 3, 1999

Using matrix-isolation infrared spectroscopy and DFT calculations, the reactions between 532 nm pulsed laser-ablated Ta and CO_2 in argon gas ambient have been investigated. The major reaction products trapped in solid argon were found to be neutral OTaCO and $O_2Ta(CO)_2$ the anions $OTaCO^-$ and $O_2Ta(CO)_2^-$. The observed absorption bands of the reaction products were identified by isotopic substitution and reproduced well by DFT calculations of vibrational fundamentals. Upon irradiation with a pulsed laser at 355 nm, the neutral OTaCO and $O_2Ta(CO)_2$ were enhanced while $O_2Ta(CO)_2^-$ and $C_2O_4^-$ anions disappeared in the measured IR spectra. The potential energy surfaces of the interactions of Ta with CO_2 and CO_2^- were calculated, and the insertion of Ta into CO_2 was suggested to proceed via electron transfer from Ta to CO_2, in which CO_2^- formation plays an important role in the activation of inert CO_2 molecules.

1. Introduction

The conversion of CO_2 into useful chemical materials has become an active field in catalytic chemistry[1−3] since carbon dioxide is the most abundant member in the C1 family. Additionally, carbon dioxide is one of the greenhouse gases and the removal of CO_2 is important from an environmental point of view. However, carbon dioxide is among the most stable triatomic molecules under normal conditions. Thus a large amount of energy input is required for CO_2 activation and conversion. Catalysts containing transition metals are probably the most promising to activate CO_2; thus, increasing attention has been paid on the reactions of transition metal atoms with CO_2 in recent years both experimentally[4−15] and theoretically.[16−20]

Recently Andrews et al.[4−9] reported the reactions of laser-ablated transition metals (M = first-row transition metals, Mo and W atoms) with CO_2 in excess argon and identified the insertion products, OMCO and $O_2M(CO)_2$ as well as η^1-C or η^1-O coordination complex by matrix-isolation IR spectroscopy and density functional calculations. These experiments indicated that photoisomerization of the OMCO molecule to form the side-bonded OM−(η^2CO) isomers and photoionization to generate the $OMCO^+$ and $OMOC^+$ cations proceed upon mercury arc photolysis. The interactions between CO_2 and transition metal centers have been studied by other research groups.[10−15] Theoretical studies on the complexes between first-row transition metals and CO_2 were also reported.[16−20] To our knowledge, investigations on the reactions between Ta and CO_2 are still lacking up to now.

In our laboratory, the composition of the plume produced by 532 nm pulsed laser ablation of a Ta target in O_2 ambient has been characterized by optical emission spectrometric,[21,22] time-of-flight mass spectrometric,[23] quadrupole mass spectrometric,[24] and matrix isolation FTIR spectroscopic techniques.[25] Both atomic and ionic Ta with high kinetic energies generated by laser ablation can easily react with O_2 to give various products such as TaO, TaO_2, $TaO_2(O_2)$, and TaO_3^-. These results imply that 532 nm pulsed laser-ablated Ta atoms are highly reactive toward small molecules.

In this work, we present studies on the reactions of 532 nm pulsed laser-ablated Ta atoms with CO_2 molecules. The MI-FTIR spectroscopic technique is employed to identify the reaction products. The structures, vibrational frequencies, and infrared intensities of the reaction products are confirmed by the effects of isotopic substitution upon the IR spectra and theoretical DFT calculations. The interactions of Ta and Ta^+ with CO_2 and CO_2^- are estimated theoretically, and the reaction mechanism of the laser-ablated Ta insertion into CO_2 and CO_2^- is proposed.

2. Experimental Details

The experimental setup is similar to that described previously.[25] A 532 nm laser beam provided by the second harmonic of a pulsed Nd:YAG laser (Spectra-Physics GCR-150) was focused onto a rotating Ta target through a hole in a CsI substrate. A gas nozzle inlet was used for introducing CO_2/Ar mixture. The laser-ablated species were co-deposited with CO_2/Ar on the CsI substrate at 11 K, which was mounted on a cold tip of a closed-cycle helium refrigerator (Air Products, model 1R02W). The deposition rate was adjusted by needle valves at a rate of ~0.7 mmol/h. The sample temperature was maintained using a temperature controller (Air Products, APD-E). IR spectra were recorded on a Bruker IFS 113v Fourier transform spectrometer equipped a Ge/KBr beam splitter and a Globar source. A spectral resolution of 0.5 cm^{-1} was used, and the number of scans ranged from 200 to 1000. The 355 nm laser beam was provided by the third harmonic output of the same Nd:YAG laser with a pulse width of 8 ns, repetition rate of 10 Hz, and laser fluence of 0.5−3 mJ/cm^2. High-purity argon and carbon dioxide (Shanghai BOC, 99.995%) and isotopic $^{13}C^{16}O_2$ (99% ^{13}C) and $^{12}C^{18}O_2 + {}^{12}C^{18}O^{16}O + {}^{12}C^{16}O_2$ (61% ^{18}O, Cambridge Isotope Laboratories) were used as received.

* Corresponding author. E-mail: qzqin@fudan.ac.cn.

10.1021/jp9927808 CCC: $19.00
Published on Web 01/06/2000

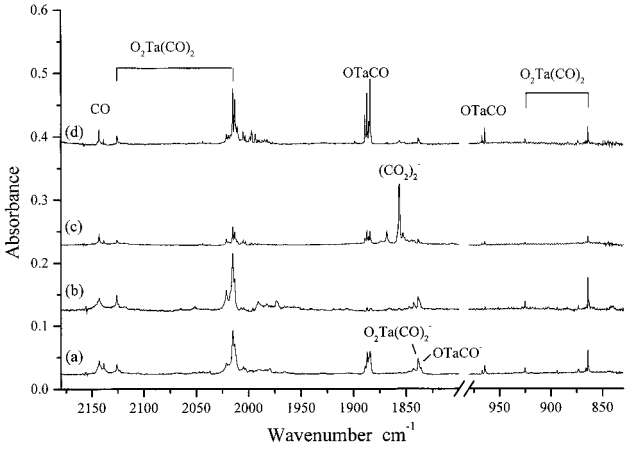

Figure 1. Infrared spectra for reaction of laser-ablated Ta with 0.2% CO_2 in excess argon and condensation at 11 K: (a) after 1 h of deposition with 3 mJ/cm^2 laser fluence; (b) after annealing to 30 K; (c) after 1 h of deposition with 0.5 mJ/cm^2 laser energy; (d) after 355 nm photolysis.

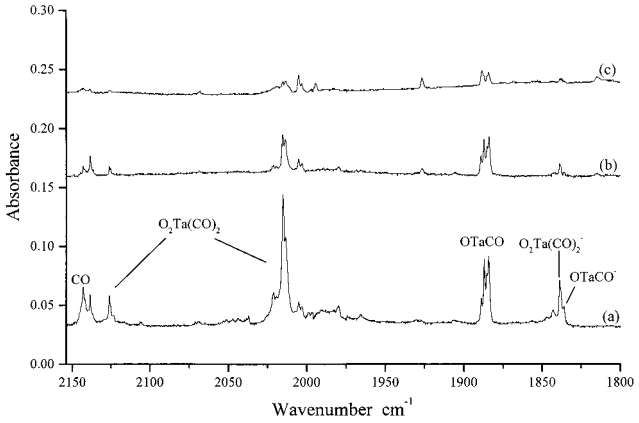

Figure 2. Infrared spectra for reaction of laser-ablated Ta with 0.2% CO_2 in excess argon doping with CCl_4 and condensation at 11 K: (a) no CCl_4 doping; (b) 0.02% CCl_4 doping; (c) 0.05% CCl_4 doping.

3. Theoretical Calculations

Density functional calculations have been performed with the Gaussian 94 programs[26] on a Power Challenge Supercomputer at Beijing, China. In our previous work[25] we examined the performance of density functionals for a set of TaO_x species and found that the B3LYP gave accurate vibrational frequencies and other molecular properties. In this work optimizations were done with the B3LYP method (Becke's nonlocal three-parameter exchange[27] with Lee−Yang−Parr correlation functional[28]). We introduced the D95* basis sets for C and O and LanL2DZ (the Los Alamos ECP plus DZ) basis sets for Ta.[29] Due to much CPU time-consuming, analytical B3LYP vibrational frequencies were calculated only for every isomer at its ground state.

The interactions of atomic Ta and Ta^+ with a linear CO_2 or a bent CO_2^- molecules were investigated in this work. Single point energy calculations were carried out with the geometries of CO_2 and CO_2^- molecules fixed at their equilibrium structures, while the distance between the midpoint of a CO bond and the metal atom varied. We think the obtained potential energy curves could at least provide a qualitative description about the nature of Ta−CO_2 interactions. The potential energy curves connecting the side-on Ta−CO_2 complexes and the insertion products were also calculated.

4. Results and Discussion

4.1. Infrared Absorption of Major Reaction Products. Infrared spectra of the products generated by the reaction of laser-ablated Ta with 0.2% CO_2 in Ar mixtures using a laser fluence of 3 mJ/cm^2 (532 nm) are shown in Figure 1. After deposition, triplets at 2126.1, 2015.7, and 2013.4 cm^{-1}, quadruplets at 1889.3, 1887.3, 1885.7, and 1884.3 cm^{-1}, and doublets at 1838.8 and 1838.1 cm^{-1} along with a 864.3 cm^{-1} band and a weak doublet at 967.3 and 964.7 cm^{-1} were observed (Figure 1a). Annealing to 30 K decreased the quadruplets at 1887.3, 1889.3, 1885.7, and 1884.3 cm^{-1} as well as doublets at 967.3 and 964.7 cm^{-1} obviously, slightly decreased the 1838.8 cm^{-1} band, and increased the triplets at 2126.1, 2015.7, and 2013.4 and the 864.3 cm^{-1} band (Figure 1b). In another experiment when a laser fluence of 0.5 mJ/cm^2 was used for ablation, very strong absorption bands assigned to $C_2O_4^-$ (1856.9 and 1184.7 cm^{-1}) and CO_2^- appeared as shown in Figure 1c; however, other bands were very weak. It indicates that laser fluence directly affects the reactions of laser-ablated metal atoms and ions with CO_2 molecules. The bands assigned to $C_2O_4^-$ and CO_2^- were completely destroyed after 355 nm laser irradiation while the intensities of the triplets and quadruplets as observed in Figure 1a grew sharply as shown in Figure 1d.

CCl_4 doping experiments were done with 0.02% and 0.05% CCl_4 added to CO_2/Ar samples. The spectra are shown in Figure 2. For 0.02% CCl_4 doping (Figure 2b), the bands at 2015.7, 1887.3, 967.3, and 864.3 cm^{-1} reduced by about 20% while the doublet at 1838.8 and 1838.1 cm^{-1} reduced by about 80%, and the absorptions of CO_2^- and $C_2O_4^-$ almost disappeared in the spectrum. However almost all of absorption bands were bleached in 0.05% CCl_4 doping (Figure 2c). The characteristic bands for the CCl_4 system[30,31] were observed at 1036.6, 897.8, 786.9, and 766.9 cm^{-1}.

For IR band identification, experiments using $^{13}C^{16}O_2$, mixed $^{13}C^{16}O_2 + {}^{12}C^{16}O_2$, and mixed $^{12}C^{18}O_2 + {}^{12}C^{16}O^{18}O + {}^{12}C^{16}O_2$ have also been done. The absorption bands exhibited isotopic shifts as listed in Table 1. The bands at 2015.7, 1887.3, and 1838.8 cm^{-1} shifted to 1907.3, 1843.8, and 1797.2 cm^{-1} when the $^{13}C^{16}O_2$ sample was used. As shown in Figures 3 and 4, mixed carbon dioxide gas samples $^{12}C^{16}O_2 + {}^{13}C^{16}O_2$ and $^{12}C^{16}O_2 + {}^{12}C^{16}O^{18}O + {}^{12}C^{18}O_2$ were used for the reaction and 355 nm laser photolysis was performed to identify the overlapped doublets at 1838.8 and 1831.8 cm^{-1}.

4.2. Theoretical Calculation Results. At the first step of our theoretical study, the potential energy curves corresponding to the interaction of atomic Ta and charged Ta^+ with linear CO_2 and bent CO_2^- were considered. The calculated results are shown in Figure 5. The interaction curves between Ta (Ta^+) and bent CO_2^- have obvious minima points, and Ta*−CO_2^- ($^5\Sigma$) also has a favorable interaction. However, the interactions of Ta (Ta^+) with linear CO_2 are essentially repulsive. This suggests that only bent carbon dioxide can serve as a good ligand bonding with metal atoms.

Second, the geometry optimizations were carried out with various initial geometries and both neutral and anion Ta(CO_2) complexes as well as insertion products were obtained. Their structures, energies, and vibrational frequencies are summarized in Table 2. We found that $^4A'$ and $^2A'$ states of neutral OTaCO are nearly degenerated with $^4A'$ state lying 1.6 kcal/mol lower in energy. The calculated frequencies of both the $^4A'$ (1967.2 and 985.5 cm^{-1}) and $^2A'$ states (1986.3 and 1012.1 cm^{-1}) are close to the experiment results, so it is difficult to determine which one is the ground state. Three electronic states of the

TABLE 1: Observed Infrared Absorptions (cm^{-1}) of Products Generated from Laser-Ablated Ta with CO_2 in Excess Argon at 11 K

molecule	CO_2	$^{13}CO_2$	$^{12}CO_2/^{13}CO_2$	$C^{16}O_2/C^{16}O^{18}O/C^{18}O_2$
OTaCO	1889.3	1845.7	1889.3, 1845.7	1889.3, 1848.0
	1887.3	1843.8	1887.3, 1843.8	1887.3, 1845.9
	1885.7	1841.6	1885.7, 1841.6	1885.7, 1844.6
	1884.3	1840.3	1884.3, 1840.3	1884.3, 1843.4
	967.3	967.3	967.3	967.3, 916.8
	964.7	964.7	964.7	964.7, 914.3
$OTaCO^-$	1838.1	1796.5	1838.1, 1796.5	1838.1, 1796.3
$O_2Ta(CO)_2$	2126.1	2078.5	2126.1, 2106.1, 2078.5	2126.0, 2106.2, 2077.7
	2015.7	1971.3	2015.2, 1988.5, 1971.3	2015.2, 1985.9, 1966.9
	2013.4	1969.5	2013.4, 1986.7, 1969.5	2013.4, 1984.2, 1965.1
	925.3	925.3	925.3	925.3, 908.5, 875.6
	864.3	864.3	864.3	864.3, 834.4, 820.9
$O_2Ta(CO)_2^-$	1838.8	1797.2	1838.8, 1814.6, 1797.2	1838.9, 1814.1, 1797.1
O_2TaCO	2005.2	1959.3	2005.2, 1959.3	2005.2, 1959.9
	2003.1	1957.4	2003.1, 1957.4	2003.1, 1959.9

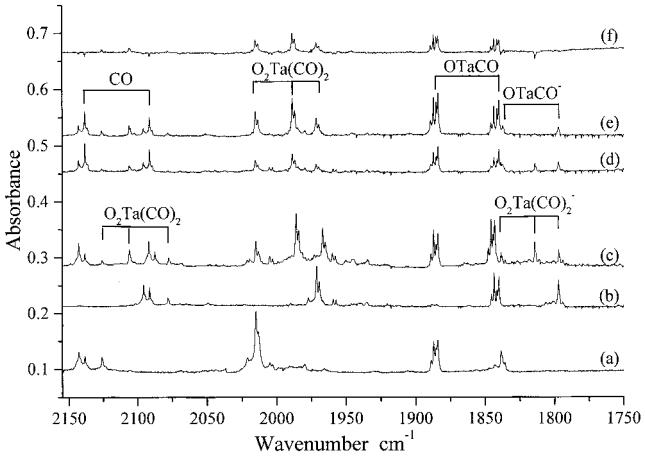

Figure 3. Infrared spectra in the 2150−1750 cm^{-1} region for reaction of laser-ablated Ta with 0.2% isotopic CO_2 samples and condensation at 11 K: (a) 0.2% $^{12}C^{16}O_2$; (b) 0.2% $^{13}C^{16}O$; (c) 0.2% $^{12}C^{16}O_2+^{12}C^{16}O^{18}O+^{12}C^{18}O_2$ (1:2:1); (d) 0.2% $^{12}C^{16}O_2+^{13}C^{16}O_2$ (1:1); (e) after 355 nm photolysis; (f) difference spectra of matrix sample before (d) and after (e) irradiation.

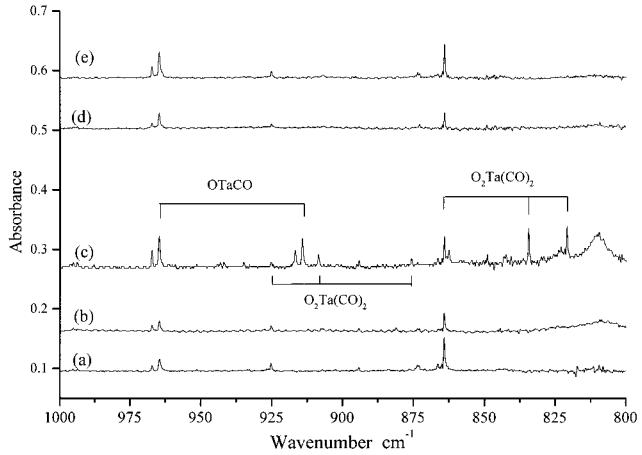

Figure 4. Infrared spectra in the 1000−800 cm^{-1} region for reaction of laser-ablated Ta with 0.2% isotopic CO_2 samples and condensation at 11 K: (a) 0.2% $^{12}C^{16}O_2$; (b) 0.2% $^{13}C^{16}O$; (c) 0.2% $^{12}C^{16}O_2$ + $^{12}C^{16,18}O_2$ + $^{12}C^{18}O_2$ (1:2:1); (d) 0.2% $^{12}C^{16}O_2$ + $^{13}C^{16}O_2$ (1:1); (e) 355 nm photolysis.

$OTaCO^-$ anion were obtained by DFT calculations. The $^1A'$ $OTaCO^-$, which is 34.9 kcal/mol lower than OTaCO ($^4A'$), is the most stable molecule among all the insertion products, indicating that the ground state of $OTaCO^-$ has minimum spin electron configurations. Other coordination complexes, such as

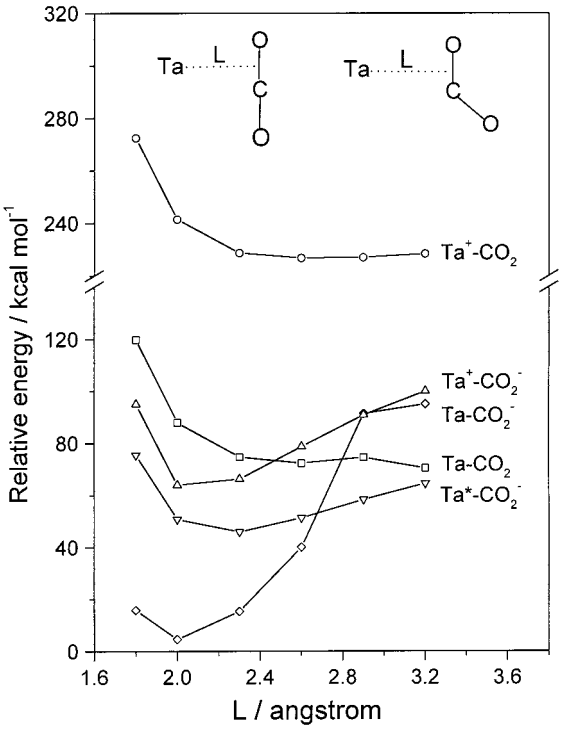

Figure 5. Interaction of Ta and Ta^+ with linear CO_2 and bent CO_2^- molecules. The structures of linear CO_2 (R = 1.18 Å) and bent CO_2^- (R = 1.26 Å, ∠OCO = 132°) are fixed, and the distance between the midpoint of the CO bond and the metal atom is varied.

Ta[η^2-OC]O, Ta[η^2-OO]C, Ta[η^2-OO]C^-, and $TaCO_2^-$, have also been located; however, their energies are much higher than the insertion product OTaCO. It should be noted that the CO_2 moieties in these complexes no longer keep a linear geometry when they coordinate to the metal atom. DFT calculations also predict that $O_2Ta(CO)_2$ (^2A) is a stable molecule while the anions with both ^1A and ^3A states are much lower in energy than the neutral species. The calculated geometric parameters, energies, and vibrational frequencies of $O_2Ta(CO)_2$ and $O_2Ta(CO)_2^-$ are listed in Table 3. These new species are first observed in our experiments and will be discussed in detail in the next section.

The potential energy surfaces for insertion processes from the adduct complexes to the final products were also calculated as shown in Figure 6. Single point energy calculations were carried out with the terminal C−O bond length fixed and other structural parameters fully optimized. The transitions from the side-on adducts to insertion products can be viewed as a consequence of rupture of the C−O bond and insertion of Ta

TABLE 2: Calculated Geometries, Energies, and Vibrational Frequencies with IR Intensities for $TaCO_2$ and $TaCO_2^-$ Isomers

molecules	tot. energy (hartree)	rel. energy (kcal/mol)	geometry (Å, deg)	freq (cm^-) (intensity, km/mol)
$OTaCO^-(^1A')$	−246.428 37	−34.9	Ta−O, 1.726; Ta−C, 2.032; CO, 1.195; ∠OTaC, 103.0; ∠TaCO, 179.6	1861.0 (909), 959.0 (128), 442.2 (2), 337.7 (0), 334.6 (33), 126.9 (2)
$OTaCO^-(^5A')$	−246.410 08	−23.4	Ta−O, 1.755; Ta−C, 2.094; CO, 1.197; ∠OTaC, 119.5; ∠TaCO, 164.8	
$OTaCO^-(^3A')$	−246.396 72	−15.0	Ta−O, 1.740; Ta−C, 2.040; CO, 1.196; ∠OTaC, 106.5; ∠TaCO, 179.0	
$OTaCO(^4A')$	−246.372 79	0.0	Ta−O, 1.714; Ta−C, 2.088; CO, 1.169; ∠OTaC, 109.8; ∠TaCO, 162.3	1967.2 (1338), 985.5 (133), 403.3 (11), 370.6 (3), 326.2 (0), 140.0 (11)
$OTaCO(^2A')$	−246.370 28	1.6	Ta−O, 1.701; Ta−C, 2.025; CO, 1.173; ∠OTaC, 96.5; ∠TaCO, 179.7	1986.3 (926), 1012.1 (102), 457.7 (3), 385.0 (8), 348.8 (1), 156.2 (9)
$Ta[OC]O'^-(^5A')$	−246.336 59	22.7	C−O′, 1.226; C−O, 1.363; Ta−O, 2.035; ∠OCO′, 126.9; ∠TaOC, 74.0	1718.6 (849), 981.3 (96), 714.2 (65), 411.2 (40), 327.9 (134), 288.7 (2)
$Ta[OO]C^-(^1A')$	−246.289 24	52.1	Ta−O, 1.950; CO, 1.384; ∠OTaO, 93.9; ∠OCO, 104.1	
$TaCO_2^-(^1B_2)$	−246.289 54	52.2	Ta−C, 2.009; C−O, 1.267; ∠TaCO, 111.9; ∠OCO, 136.2	1326.0 (531), 978.7 (239), 691.8 (11), 413.5 (3), 322.2 (9), 295.3 (38)
$Ta[OC]O'(^4A')$	−246.284 53	55.4	C−O′, 1.199; C−O, 1.387; Ta−O, 1.960; ∠OCO′, 129.7; ∠TaOC, 74.6	1669.9 (312), 1224.6 (297), 739.3 (98), 494.3 (3), 480.3 (1), 329.4 (3)
$Ta[OC]O'(^6A')$	−246.247 53	78.6	C−O′, 1.199; C−O, 1.264; Ta−O, 2.161; ∠OCO′, 145.4; ∠TaOC, 68.8	
$Ta[OO]C(^2A')$	−246.223 85	93.4	Ta−O, 1.946; CO, 1.367; ∠OTaO, 90.9; ∠OCO, 108.7	
$Ta[OO]C^-(^5A')$	−246.218 44	96.8	Ta−O, 2.308; CO, 1.257; ∠OTaO, 88.8; ∠OCO, 124.7	
$TaCO_2^-(^5B_2)$	−246.193 46	112.5	Ta−C, 2.009; C−O, 1.267; ∠TaCO, 111.9; ∠OCO, 136.2	
$Ta[OO]C(^4A')$	−246.180 74	120.5	Ta−O, 2.201; CO, 1.262; ∠OTaO, 89.7; ∠OCO, 120.8	

TABLE 3: Calculated Geometries, Energies, Vibrational Frequencies, and IR Intensities for $O_2Ta(CO)_2$, $O_2Ta(CO)_2^-$, and O_2TaCO

molecules	tot. energy (hartree)	rel. energy (kcal/mol)	geometry (Å, deg)	freq (cm^-) (intensity, km/mol)
$O_2Ta(CO)_2(^2\Sigma)$	−435.083 96	0.0	C−O, 1.148; Ta−C, 2.212; Ta−O, 1.750; ∠OCTa, 174.1; ∠CTaC, 104.6; ∠OTaO, 109.8	2165.2 (236), 2063.5 (2179), 961.6 (51), 901.3 (183), 365.2 (5), 342.4 (7), 331.6 (16), 326.8 (7), 324.6 (0), 317.1 (202), 269.0 (7), 106.1 (0), 94.7 (21), 73.6 (5), 52.5 (0)
$O_2Ta(CO)_2^-(^3A)$	−435.137 86	−33.8	C−O, 1.183; Ta−C, 2.215; Ta−O, 1.782; ∠OCTa, 174.4; ∠CTaC, 109.9; ∠OTaO, 109.4	
$O_2Ta(CO)_2^-(^1\Sigma)$	−435.186 76	−64.5	C−O, 1.174; Ta−C, 2.121; Ta−O, 1.789; ∠OCTa, 174.6; ∠CTaC, 91.4; ∠OTaO, 110.3	2019.6 (428), 1923.7 (1888), 899.3 (71), 841.2 (253), 499.4 (6), 419.9 (0), 406.9 (6), 398.7 (8), 371.5 (0), 365.7 (10), 238.4 (12), 132.3 (14), 127.3 (0), 97.9 (5), 69.0 (0)
$O_2TaCO(^2A)$	−321.700 75		C−O, 1.155; Ta−C, 2.171; Ta−O, 1.739; ∠OCTa, 163.2; ∠OTaO, 103.6; ∠CTaC, 109.9	2054.0 (1821), 979.0 (49), 916.0 (183), 357.2 (17), 332.7 (1), 301.5 (2), 287.3 (13), 117.0 (26), 101.5 (1)

to form the new O−Ta−CO bond. It can be seen that the energy barrier for conversion of Ta[η^2-OC]O^- to $OTaCO^-$ is about 10 kcal/mol (Figure 6, lower curve); however, a much smaller barrier of about 1 kcal/mol is obtained for the neutral species (Figure 6, upper curve).

4.3. Assignments. OTaCO. The strong bands at 1887.3 and 967.3 cm^{-1} exhibit the same behavior throughout annealing, photolysis, and CCl_4 doping experiments, suggesting that they are due to different vibrational modes of a same molecule. When the $^{13}C^{16}O_2$ sample was used, the 1887.3 cm^{-1} bands shifted to 1843.8 cm^{-1}, and the $^{12}C/^{13}C$ isotopic ratio (1.02393) is close to that for the C−O stretching vibration. This band is 264.9 cm^{-1} lower than the CO monomer frequency in solid argon. The doublet structure in both the mixed $^{12}C^{16}O_2 + {}^{13}C^{16}O_2$ and $^{12}C^{16}O_2 + {}^{12}C^{16}O^{18}O + {}^{12}C^{18}O_2$ experiments (Figure 3) indicates that only one CO subunit is involved in this mode. The 967.3 cm^{-1} band exhibited no carbon-13 isotopic shift but showed a 1:1 doublet (967.3 and 916.8 cm^{-1}) using the $^{12}C^{16}O_2 + {}^{12}C^{16}O^{18}O + {}^{12}C^{18}O_2$ sample (Figure 4). The frequency and 16/18 isotopic ratio (1.02243) are very close to those of the diatomic TaO molecule in solid argon.[32] This evidence suggests that the 967.3 cm^{-1} band should be assigned to a terminal Ta−O stretching vibration. These facts support the assignment of the two bands at 1887.3 and 967.3 cm^{-1} to the inserted OTaCO molecule.

This assignment is in good agreement with our DFT calculations. The B3LYP calculation predicts that OTaCO in the $^4A'$ ground state is the most stable $TaCO_2$ isomer. The TaO and CO bond lengths are 1.71 and 1.17 Å, respectively, which are close to those of free TaO and CO molecules. The Ta−C bond length (2.09 Å) is rather long and the O−Ta−C angle is about 110°, suggesting that the molecule is like a complex between CO and TaO. The B3LYP calculation gives 985.5 cm^{-1} Ta−O and 1967 cm^{-1} C−O stretching frequencies, which are slightly higher than the experimental values (967.3 and 1889.3 cm^{-1}). As can be seen from Table 2, the calculated relative intensities for both Ta−O and C−O modes, as well as the calculated isotopic ratio for the C−O mode (1.02325), match the observed value (1.02393) well. Obviously, DFT calculations satisfactorily characterize the observed OTaCO molecule and its normal modes.

TABLE 4: Comparison of Observed and Calculated Vibrational Frequencies (cm^{-1}) and Isotopic Frequencies Ratios of Reaction Products

			$^{12}C/^{13}C$		$^{16}O/^{18}O$	
molecule	obsd	calcd	obsd	calcd	obsd	calcd
$OTaCO(^4A')$	1887.3	1967.2	1.023 93	1.023 25	1.022 43	1.024 06
	967.3	985.5	1.000 00	1.000 00	1.055 08	1.055 48
$OTaCO^-(^1A')$	1838.1	1861.0	1.023 16	1.024 22	1.023 27	1.022 58
$O_2Ta(CO)_2(^2\Sigma)$	2126.1	2165.2	1.022 95	1.023 44	1.023 34	1.023 40
	2015.7	2063.5	1.022 27	1.022 85	1.024 66	1.024 58
	925.3	961.6	1.000 00	1.000 00	1.056 76	1.057 75
	864.3	901.3	1.000 00	1.000 00	1.052 87	1.054 15
$O_2Ta(CO)_2^-(^1\Sigma)$	1965.9	2019.6	1.023 53	1.024 11	1.023 69	1.022 84
	1838.8	1923.7	1.023 15	1.023 57	1.023 26	1.023 54
	809.6	841.2	1.000 00	1.000 00	?	1.052 57
$O_2TaCO(^2A)$	2005.2	2054.0	1.023 43	1.023 11	1.023 11	1.024 23

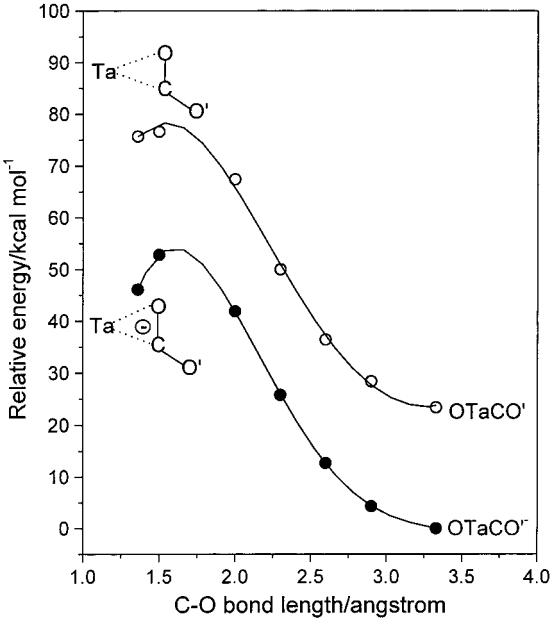

Figure 6. Plot of energy versus C−O bond length. The energy curves link the adduct complexes and the insertion products.

$O_2Ta(CO)_2$. The other group of strong bands appearing at 2126.1, 2015.7, 925.3, and 864.3 cm^{-1} can be assigned to the $O_2Ta(CO)_2$ molecule. Using the $^{13}C^{16}O_2$ sample, two bands in the C−O stretching region (2126.1 and 2015.7 cm^{-1}) shifted to 2078.5 and 1971.3 cm^{-1} while the bands at 925.3 and 864.3 cm^{-1} in the O−Ta−O symmetric and antisymmetric stretching region[25,32] showed no apparent shifts, which indicate that carbon atom is not involved in these modes. The mixed $^{12}C^{16}O_2 + ^{13}C^{16}O_2$ (1:1) sample (Figures 3d and 4d) gave 1:2:1 triplets for the modes attributed to C−O symmetric and antisymmetric vibrations, but the modes attributed to the OTaO moiety (925.3 and 864.3 cm^{-1}) are not shifted. It confirms that two equivalent CO groups and two equivalent oxygen atoms are bonded to one Ta atom. The experiments with $^{12}C^{16}O_2 + ^{12}C^{16}O^{18}O + ^{12}C^{18}O_2$ mixtures (Figures 3c and 4c) resulted in a 1:2:1 isotopic triplet for both CO stretching modes and OTaO symmetric and antisymmetric stretching fundamentals. DFT calculations also reproduce the frequencies and isotopic shifts of $O_2Ta(CO)_2$ well as shown in Tables 3 and 4. Both observed and calculated frequencies and isotopic ratios confirmed the identification of the $O_2Ta(CO)_2$ molecule.

$OTaCO^-$ and $O_2Ta(CO)_2^-$. A relatively strong band at 1838.8 cm^{-1} with a shoulder at 1838.1 cm^{-1} was observed in the IR spectra as shown in Figures 1a and 3a. The 1:2:1 triplet isotopic structure in the $^{12}C^{16}O_2 + ^{12}C^{16}O^{18}O + ^{12}C^{18}O_2$ experiments indicated that the bands are due to two terminal C−O stretching vibrations (Figure 3c). However the $^{12}C^{16}O_2 + ^{13}C^{16}O_2$ (1:1) experiment gave a 1:1:1 triplet isotopic structure (Figure 3d). After irradiation with 355 nm laser the band at 1814.6 cm^{-1} vanished, while the other two bands at 1838.8 and 1797.2 cm^{-1} changed slightly (Figure 3e). These results clearly showed that this set of bands includes the contributions from two species, one with two and the other with only one terminal CO. The species with two terminal CO groups was destroyed completely by the 355 nm laser photolysis. The CCl_4 doping experiments using different concentrations of CCl_4 showed that these bands decreased more substantially than the bands of the neutral species as CCl_4 concentration increased (Figure 2). This implies that all these absorptions should be attributed to anions.

The species with two terminal CO should be assigned to the $O_2Ta(CO)_2^-$ anion. The ground state of $O_2Ta(CO)_2^-$ is $^1A'$ in the B3LYP calculations. As shown in Table 3, $O_2Ta(CO)_2^-$ ($^1A'$) is 64.5 kcal/mol lower in energy than its neutral isomer. The band at 1838.8 cm^{-1} exhibited terminal C−O stretching vibrational isotopic ratios, and triplets were observed in both $^{12}C^{16}O_2 + ^{13}C^{16}O_2$ and $^{12}C^{16}O_2 + ^{12}C^{16}O^{18}O + ^{12}C^{18}O_2$ spectra. The weak band at 1965.9 cm^{-1} is tentatively assigned to the asymmetric stretching mode of CO moieties in $O_2Ta(CO)_2^-$, and the weak band at 809.6 cm^{-1} is most likely the asymmetric stretching mode of OTaO in $O_2Ta(CO)_2^-$. Unfortunately, these bands are too weak for observing any isotope structures. As can be seen from Tables 3 and 4, the calculated frequencies reproduce the observed spectra well for $O_2Ta(CO)_2^-$.

The species with one terminal CO should be assigned to the $OTaCO^-$ anion, and DFT calculations confirmed the assignments. As listed in Table 2, the B3LYP calculations locate three states of $OTaCO^-$ isomers. The $^1A'$ state is the most stable one, which is 34.9 kcal/mol lower in energy than neutral OTaCO. The calculated vibrational frequencies and isotopic frequencies ratios are in excellent agreement with the experimental values. The Ta−O stretching mode of $OTaCO^-$ was not observed here since this mode was estimated to be very weak compared to the C−O stretching vibration.

O_2TaCO. The band at 2005 cm^{-1} slightly reduced upon 355 nm laser photolysis. Doublet features were observed in mixed $^{12}C^{16}O_2 + ^{13}C^{16}O_2$ and $^{12}C^{16}O_2 + ^{12}C^{16}O^{18}O + ^{12}C^{18}O_2$ experiments, implying that only one CO subunit is involved in this mode. The 2005 cm^{-1} band is close to the C−O stretching mode predicted for O_2TaCO (see Table 3 for geometry and frequencies). Moreover, the isotopic ratios are also very close (see Table 4) so we tentatively assign this band to O_2TaCO. The calculated intensities of the TaO_2 stretching modes are relatively weak which explains the absence of these bands in our spectra.

4.4. Reaction Mechanism. The above experimental evidence and theoretical analysis suggest a reasonable reaction mechanism

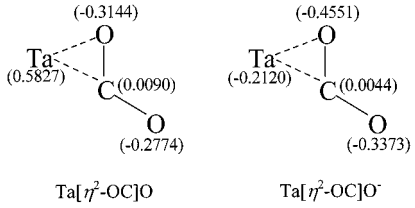

Figure 7. Atomic charge distributions for Ta[η^2-OC]O and the Ta[η^2-OC]O^- anion.

for the insertion of laser-ablated Ta into the C−O bond of the CO_2 molecule. In the first step, the interaction of a short-pulsed laser beam with a Ta target will produce a plasma plume, which contains energetic electrons, neutral atoms, and positive ions in both ground and excited states.[21−24] The neutral CO_2 molecules can trap electrons to form anions through reactions 1 and 2.

$$CO_2 + e \rightarrow CO_2^- \quad (1)$$

$$2CO_2 + e \rightarrow C_2O_4^- \quad (2)$$

Then atomic Ta or Ta^+ can react with both neutral CO_2 and the anion CO_2^-. Let us consider the OTaCO formation channel first. To simplify the insertion process, only the ground state of Ta is considered. The formation of M−CO_2 complexes can be supposed as a primary step in the activation process of the inert CO_2 molecule.[1−3,33] Our calculation results showed that the interaction of the ground-state Ta atom with CO_2 can form various complexes, Ta[η^2-OC]O, Ta−CO_2, and Ta[η^2-OO]C, in which side-on Ta[η^2-OC]O is lowest in energy. As can be seen from the Mulliken populations of Ta[η^2-OC]O shown in Figure 7, the Ta atom is positively charged while the CO_2 moiety, which is similar to the free CO_2^- radical, retains negative charge. As shown in Figure 5, the interactions of Ta^+ with bent CO_2^- (curve Ta^+−CO_2^-) are more favorable than that of the Ta atom with linear CO_2 (curve Ta−CO_2) to form the side-on Ta[η^2-OC]O complex, which converts to the insertion product OTaCO easily via reaction 3.

$$Ta^+ + CO_2^- \rightarrow Ta[\eta^2\text{-OC}]O \rightarrow OTaCO \quad (3)$$

As can be seen from the potential energy curves in Figure 6, the insertion energy barrier from Ta[η^2-OC]O to OTaCO is only about 1 kcal/mol. It implies that the formation of OTaCO is favorable but Ta[η^2-OC]O complex is unstable and could not be isolated in an Ar matrix. However, the Ta[η^2-OC]O complex might be tentatively formed during interaction of atomic Ta with the linear CO_2 molecule if charge transfer from the Ta atom to the CO_2 molecule would occur. It is possible that laser-ablated atomic Ta with high kinetic energies could attack the linear CO_2 molecule and induce the charge transfer to form an adduct complex which then converts to OTaCO. Excess CO_2 molecules and Ta atoms could be trapped in the Ar matrix after deposition; however, the intensities of OTaCO absorptions remained unchanged during annealing (Figure 1b), indicating that the insertion reaction is not favored under such conditions.

Formation of the Ta−CO_2 adducts is crucial for subsequent insertion reaction, and we believe that only hot Ta atoms in the gas phase can approach the CO_2 molecule and induce charge transfer. In the experiment using lower laser fluence (0.5 mJ/cm^2), the ablated electrons can attach to CO_2 molecules to form the $C_2O_4^-$ and CO_2^- anions, but the laser-ablated Ta atoms have relatively low kinetic energies as well as a low concentration in the plume. They could not easily react with other reaction partners (CO_2, $C_2O_4^-$, and CO_2^-) due to lower reactivity. As a result the major products are $C_2O_4^-$ and CO_2^- and the Ta-containing species were with very low intensities as shown in Figure 1c.

Another reaction channel considered is $OTaCO^-$ anion formation. When the laser ablation process occurs in ambient CO_2, the primary energetic electrons can be captured by CO_2 to generate the CO_2^- anion since CO_2 is a relatively strong acceptor of electrons. The atomic Ta can combine with CO_2^- to form a Ta[η^2-OC]O^- intermediate. DFT calculations also predict this anion to be a stable complex, and its binding energy relative to the ground-state species ($Ta(s^2d^3) + CO_2^-$ (^2A)) is estimated to be 68 kcal/mol. Atomic charge distributions for the Ta[η^2-OC]O^- anion (Figure 7) show that both O atoms and Ta atoms possess negative partial charge but the C atom has a partial positive charge, which may influence the stability of this species. Breakage of the C−O bond in Ta[η^2-OC]O^- to form $OTaCO^-$ is also energetically favorable (exothermic by 46.1 kcal/mol), but reaction 4 has an energy barrier of about 10 kcal/mol as shown in Figure 6.

$$Ta + CO_2^- \rightarrow Ta[\eta^2\text{-OC}]O^- \rightarrow OTaCO^- \quad (4)$$

Our experimental results also showed that 0.05% CCl_4 doping prohibited the generation of all products, implying that electrons play an important role in the reaction process. It is reasonable that CCl_4 as an electron-trapping agent greatly affects the electron transfer in reaction 3 and formation of CO_2^- in reaction 1. So almost all the insertion products were eliminated in the CCl_4 doping experiments.

Besides the formations of OTaCO and $OTaCO^-$ from Ta insertion reactions as mentioned above, the insertion product $O_2Ta(CO)_2$ increased at the expense of OTaCO on annealing. It indicates that OTaCO can easily react with trapped CO_2 with no distinct activation energy, and $O_2Ta(CO)_2$ is expected to be formed by reaction 5.

$$OTaCO + CO_2 \rightarrow O_2Ta(CO)_2 \quad (5)$$

This reaction was calculated to be exothermic by 55.6 kcal/mol, suggesting that insertion reaction of OTaCO into CO_2 is thermodynamically very favorable.

5. Conclusions

Reactions of laser-ablated Ta species with CO_2 molecules result in the insertion products including the neutral OTaCO and $O_2Ta(CO)_2$ and $OTaCO^-$ and $O_2Ta(CO)_2^-$ anions. These species are identified by matrix-isolation FTIR spectroscopy. The structures and vibrational assignments are confirmed by means of ^{13}C- and ^{18}O-enriched experiments and by comparing with the B3LYP theoretical calculations. The potential energy curves of interactions between atomic Ta with CO_2 and CO_2^- show that the electron transfer from Ta to CO_2 and the formation of CO_2^- are important in activation of inert CO_2 molecules. We also found that OTaCO could activate CO_2 molecules to form $O_2Ta(CO)_2$, and the insertion process has no activation energy.

Acknowledgment. The authors thank Professor Qi-ke Zheng and Dr. Zhou Mingfei for helpful discussions. This work is supported by the Climbing Project of China.

References and Notes

(1) Braunstrin, P.; van Dldik, R. *Chem. Rev.* **1982**, *11*, 57.
(2) Cutler, A. R.; Hanna, P. K.; Vites, J. C. *Chem. Rev.* **1988**, *88*, 1363.

(3) Gibson, D. H. *Chem. Rev.* **1996**, *96*, 2063.
(4) Zhou, M. F.; Andrews, L. *J. Phys. Chem. A* **1999**, *103*, 2066.
(5) Zhou, M. F.; Liang, B. Y.; Andrews, L. *J. Phys. Chem. A* **1999**, *103*, 2013.
(6) Zhou, M. F.; Chertihin, G. V.; Andrews, L. *J. Chem. Phys.* **1999**, *109*, 10893.
(7) Zhou, M. F.; Andrews, L. *J. Am. Chem. Soc.* **1998**, *120*, 13230.
(8) Souter, P. S.; Andrews, L. *J. Am. Chem. Soc.* **1997**, *119*, 7350.
(9) Chertihin, G. V.; Andrews, L. *J. Am. Chem. Soc.* **1995**, *117*, 1595.
(10) Sievers, M. R.; Armentrout, P. B. *J. Chem. Phys.* **1995,** *102*, 754.
(11) Schwartz, J.; Heinemann, C.; Schwartz, H. *J. Phys. Chem.* **1995**, *99*, 11405.
(12) Schwartz, J.; Schwartz. H. *Organometallics* **1994**, *13*, 1518.
(13) Asher, R. L.; Bellert, D.; Buthelezi, T,; Brucat, P. J. *Chem. Phys. Lett.* **1994**, *227*, 623.
(14) Lessen, D. E.; Asher, R. L.; Brucat, P. J. *J. Phys. Chem. A* **1991**, *95*, 1414.
(15) Mascetti, J.; Tranquille, M. *J. Phys. Chem. A* **1988**, *92*, 2173.
(16) Papai, I.; Mascetti, J,; Fournier, R. *J. Phys. Chem. A* **1997**, *101*, 4465.
(17) Galan, F.; Fouassier, M.; Tranquille, M.; Mascetti, J.; Papai, I. *J. Phys. Chem. A* **1997**, *101*, 2626.
(18) Sodupe, M.; Branchadell, V.; Rosi, M.; Bauschlicher, C. W., Jr. *J. Phys. Chem. A* **1997**, *101*, 7854.
(19) Jeung, G. H. *Chem. Phys. Lett.* **1995**, *232*, 319.
(20) Sodupe, M.; Branchadell, V.; Oliva, A. *J. Phys. Chem.* **1995**, *99*, 8567.
(21) Zhou, M. F.; Fu, Z. W.; Qin, Q. Z. *Appl. Surf. Sci.* **1998**, *125*, 208.
(22) Fu, Z. W.; Zhou, M. F.; Qin, Q. Z. *Appl. Phys. A* **1997**, *65*, 445.
(23) Wang, X.; Gu, Z.; Qin, Q. Z. *Int. J. Mass Spectrom.* **1999**, *188*, 205.
(24) Qin, Q. Z.; Han, Z. H.; Dang, H. J. *J. Appl. Phys.* **1998**, *83*, 6082.
(25) Chen, M.; Wang, X.; Zhang, L.; Yu, M.; Qin, Q. Z. *Chem. Phys.* **1999**, *242*, 81.
(26) Frisch, M. J.; Trucks, G. W.; Schlegel, H. B.; Gill, P. M. W.; Johnson, B. G.; Robb, M. A.; Cheeseman, J. R.; Keith, T.; Petersson, G. A.; Montgomery, J. A.; Raghavachari, K.; Al-Laham, M. A.; Zakrzewski, V. G.; Ortiz, J. V.; Foresman, J. B.; Cioslowski, J.; Stefanov, B. B.; Nanayakkara, A.; Challacombe, M.; Peng, C. Y.; Ayala, P. Y.; Chen, W.; Wong, M. W.; Andres, J. L.; Replogle, E. S.; Gomperts, R.; Martin, R. L.; Fox, D. J.; Binkley, J. S.; Defrees, D. J.; Baker, J.; Stewart, J. P.; Head-Gordon, M.; Gonzalez, C.; Pople, J. A. *Gaussian 94*, *Revision D.3*; Gaussian, Inc.: Pittsburgh, PA, 1995.
(27) Becke, A. D. *J. Chem. Phys.* **1993**, *98*, 5648.
(28) Lee, C.; Yang, R. G.; Parr, R. G. *Phys. Rev. B* **1988**, *37*, 785.
(29) Hay, P. J.; Wadt, W. R. *J. Chem. Phys.* **1985**, *82*, 299.
(30) Menberger, L. *Ber. Bunsen-Ges. Phys. Chem.* **1982**, *86*, 252.
(31) Prochaska, F. T.; Andrews, L. *J. Chem. Phys.* **1977**, *67*, 1091.
(32) Zhou, M. F.; Andrews, L. *J. Phys. Chem. A* **1998**, *102*, 8251.
(33) Braunstein, P.; Matt, D.; Nobel, D. *Chem. Rev.* **1988**, *88*, 747.